A nitrate transporter 1/peptide transporter family gene impacts nitrogen homeostasis and phenylpropanoid production in hybrid poplar

Lan T. Tran, Yaseen Mottiar, Tyler Irwin, Mahinur Efe, Samantha Robbins, Barbara J. Hawkins, Shawn D. Mansfield, & Jürgen Ehlting

2026

Original citation:
Tran, L. T., Mottiar, Y., Irwin, T., Efe, M., Robbins, S., Hawkins, B. J., Mansfield, S. D., & Ehlting, J. (2026). A nitrate transporter 1/peptide transporter family gene impacts nitrogen homeostasis and phenylpropanoid production in hybrid poplar. *Journal of Experimental Botany*, *77*(5), 1483–1493.
https://doi.org/10.1093/jxb/erag034

Journal of Experimental Botany, Vol. 77, No. 5 pp. 1483–1493, 2026
https://doi.org/10.1093/jxb/erag034 Advance Access Publication 3 February 2026

BRIEF COMMUNICATION

A nitrate transporter 1/peptide transporter family gene impacts nitrogen homeostasis and phenylpropanoid production in hybrid poplar

Lan T. Tran[1,2], Yaseen Mottiar[3,4], Tyler Irwin[1], Mahinur Efe[1], Samantha Robbins[1], Barbara J. Hawkins[1], Shawn D. Mansfield[2,3], and Jürgen Ehlting[1,*]

[1] Centre for Forest Biology & Department of Biology, University of Victoria, Victoria, BC V8W 2Y2, Canada
[2] Department of Botany, University of British Columbia, Vancouver, BC V6T 1Z4, Canada
[3] Department of Wood Science, University of British Columbia, Vancouver, BC V6T 1Z4, Canada
[4] Department of Biology, University of Ottawa, Ottawa, ON K1N 6N5, Canada

* Correspondence: je@uvic.ca

Received 30 April 2025; Accepted 16 January 2026

Editor: Vanessa Wahl, The James Hutton Institute, UK

Abstract

In plants, nitrogen and carbon metabolism are tightly interconnected, and nitrogen availability often negatively correlates with phenylpropanoids that are associated with xylem formation and stress responses. A nitrate transporter 1/peptide transporter (NRT1/PTR) family (NPF) gene (*PtNPF6.1*), which is expressed in the vasculature, was previously found to have a genetic association with the variation in syringyl lignin content in poplar trees (*Populus trichocarpa*). PtNPF6.1 belongs to an evolutionarily distinct NPF superfamily with limited taxonomic distribution. RNAi-mediated suppression of *PtNPF6.1* led to increases in total foliar nitrogen and amino acids related to nitrogen transport and storage in source leaves. There was also a concomitant decrease in soluble phenolics, including attenuated stress-induced production of anthocyanins and condensed tannins. The proportions of syringyl and *p*-hydroxyphenyl units in lignin were slightly but significantly decreased in down-regulated lines grown under high nitrogen conditions, while there was an increase in the level of ester-linked *p*-hydroxybenzoate groups. Together, these results suggest that PtNPF6.1 is involved in maintaining internal nitrogen homeostasis in trees, indirectly impacting the production of nitrogen-free phenolics including lignin and soluble secondary metabolites.

Keywords: Amino acids, fertilization, high light, lignin, nitrate, nitrogen transport, peptide, phenolics, phenylpropanoids, poplar.

Introduction

Nitrogen (N) is an essential macronutrient for plant growth and development, most notably as a component of nucleic acids, amino acids, chlorophyll, and certain classes of secondary metabolites (Cantón *et al.*, 2005; Parker and Newstead, 2014). Some non-N-containing secondary metabolites, such as the phenylpropanoids, nevertheless require N-containing precursors in the form of phenylalanine (Phe) (Razal *et al.*, 1996; Vogt, 2010). N can be acquired from the soil in an inorganic form, mainly as nitrate

(NO_3^-) or ammonium (NH_4^+), or as organic N in the form of amino acids and/or peptides (Paungfoo-Lonhienne *et al.*, 2008; Wang *et al.*, 2012). Compared with the annual model plant Arabidopsis (*Arabidopsis thaliana*), N transport has been less extensively studied in woody perennials, despite N being a growth-limiting nutrient in many forest ecosystems (Castro-Rodríguez *et al.*, 2017). Trees such as poplar are highly responsive to environmental N availability (Cooke *et al.*, 2003; Geβler *et al.*, 2004; Rennenberg *et al.*, 2010; Luo *et al.*, 2013). Under N-rich conditions, poplars increase shoot biomass relative to roots and modify xylem anatomy and cell wall chemistry, producing thinner walled fibres, wider vessels, and lignin with a reduced proportion of syringyl subunits (Pitre *et al.*, 2007a, b; Plavcová *et al.*, 2013; Euring *et al.*, 2014). In parallel, the accumulation of soluble phenolics, including anthocyanins and condensed tannins, is influenced by N availability (e.g. Larbat *et al.*, 2012; Gourlay and Constabel, 2019). These responses are consistent with the protein competition model of phenolic allocation (Jones and Hartley, 1999), which proposes that photosynthates are preferentially allocated to protein biosynthesis for growth under N-sufficient conditions, but diverted towards phenolics and other N-free compounds for defence and structural rigidity under N limitation.

In plants, diverse families of transporters facilitate the uptake, translocation, and remobilization of inorganic and organic N (reviewed in Masclaux-Daubresse *et al.*, 2010). Among these, the nitrate transporter 1/peptide transporter (NRT1/PTR) family (NPF) is particularly large and functionally diverse (Léran *et al.*, 2014). Arabidopsis NPFs are the best characterized, with nearly two-thirds of the 53 identified *NPF* genes having been studied (reviewed in Tsay *et al.*, 2007; Corratgé-Faillie and Lacombe, 2017). Many Arabidopsis NPFs transport nitrate and function in root uptake, vascular loading/unloading, and maintenance of N homeostasis in leaves (Tsay *et al.*, 1993; Huang *et al.*, 1996, 1999; Chiu *et al.*, 2004; Lin *et al.*, 2008). A smaller subset, including NPF8.1/PTR1 and NPF8.2/PTR5, mediate long-distance transport of di- and tripeptides (Dietrich *et al.*, 2004; Komarova *et al.*, 2008). More recently, an increasing number of NPF members have been shown to transport hormones and secondary metabolites, including phenylpropanoids (Kanno *et al.*, 2012; Nour-Eldin *et al.*, 2012; Tal *et al.*, 2016; Payne *et al.*, 2017; Grunewald *et al.*, 2020; Binenbaum *et al.*, 2023).

Genome-wide surveys have identified between 67 and 70 *NPF* genes in black cottonwood (*Populus trichocarpa*), organized into distinct phylogenetic groups (Bai *et al.*, 2013; Léran *et al.*, 2014; von Wittgenstein *et al.*, 2014), yet none has been functionally characterized to date. Because poplar can acclimate to a range of N forms and produces a diverse set of phenolic compounds (Min *et al.*, 2000; Mellway *et al.*, 2009; Renström *et al.*, 2024), it provides an excellent system for investigating N-related transport mechanisms and the influence of N on phenolic metabolism.

A large-scale genetic association study in *P. trichocarpa* identified an *NPF* gene (named *PtNPF6.1* here) associated with natural variation in syringyl lignin content (Porth *et al.*, 2013a), providing an opportunity to investigate N-related genes not previously connected to phenolic metabolism. Here, we used a reverse genetics approach to characterize *PtNPF6.1*. Reporter gene analysis revealed *PtNPF6.1* expression primarily in vascular tissues, while RNAi-mediated suppression increased total foliar N and decreased phenolic compounds. Under N-rich conditions, *PtNPF6.1* RNAi lines exhibited a modest reduction of syringyl lignin content. This suggests that PtNPF6.1 influences carbon (C) allocation between proteins and phenolics by mediating the internal mobilization of N-containing compounds within vascular tissues.

Materials and methods

Phylogenetic tree construction

Using PtNPF6.1 (Potri.002G029200) as a bait for BLASTp searches, all hits with at least 50% sequence identity (if present), or the single best hit (regardless of sequence similarity), were initially retained. The 50% threshold was selected because previously reported supergroup J members, as described in von Wittgenstein *et al.* (2014), were >60% identical to PtNPF6.1, while NPFs from other supergroups were <50% identical. Searches were performed against NCBI Genbank (Benson *et al.*, 2017) separately for each major taxonomic lineage within the *Viridiplantae* to assess the presence or absence in each lineage, whole genomes present in Phytozome v12.1 (Goodstein *et al.*, 2012), and the 1KP transcriptome database (One Thousand Plant Transcriptomes Initiative, 2019).

To generate a backbone phylogeny of the NPF superfamily, all NPF sequences from *P. trichocarpa* and *Mimulus guttatus* (representing Rosid and Asterid eudicots), *Brachypodium distachyon* and *Setaria viridis* (representing C_3 and C_4 monocots), *Selaginella moellendorffii* (representing lycopods), and *Physcomitrium patens* (representing bryophytes) were retained from our previous collection (von Wittgenstein *et al.*, 2014). Sequences were aligned using Clustal W v1.4 (Thompson *et al.*, 1994) and used for initial distance Neighbor–Joining phylogenies. Since we aimed to expand the phylogeny for only supergroup J, new sequences that grouped into the other supergroups were removed from the alignment. This included all sequences with <50% sequence identity that were initially retained from the original BLAST searches. We defined supergroups as separation events prior to the bryophyte/vascular plant split, as described by von Wittgenstein *et al.* (2014). Therefore, for supergroup J, the clade is defined by the monilophyte (fern) sequences at its base since bryophyte sequences were not identified. The final sequence dataset was again aligned using Clustal W and was trimmed based on the transitive consistency score (TCS) obtained from the T-Coffee web service (http://tcoffee.crg.cat/tcs) (Chang *et al.*, 2015) using default settings, which removes alignment columns with a TCS of <4. A maximum likelihood phylogeny was reconstructed using PhyML v3.0 at the ATGC web server (http://www.atgc-montpellier.fr/phyml) (Guindon *et al.*, 2010). Based on 'Smart Model Selection' (Lefort *et al.*, 2017), the LG model was used, and branch support was assessed using the non-parametric approximate likelihood ratio test based on a Shimodaira–Hasegawa-like procedure. Tree visualization was achieved using FigTree (http://tree.bio.ed.ac.uk/software/figtree). The complete sequence collection, including accession numbers, is provided as Supplementary Table S1.

Plant maintenance and stress treatments

Hybrid aspen (*Populus tremula* × *P. alba*) clone INRA 717-1B4 was maintained under sterile conditions in Magenta GA-7 plant tissue culture vessels on solid half-strength Murashige and Skoog (MS) basal medium

(PhytoTechnology Laboratories) supplemented with 0.5 μg ml^{-1} indole butyric acid (IBA) and grown in a plant tissue culture chamber (Caron) under long-day conditions (16 h light, 8 h dark) at 22 °C. For all experiments, tissue culture plantlets, 5–10 cm in height, were transferred to Sunshine Mix #4 (Sun Gro Horticulture), a peat-based growing mix, and moved to a greenhouse (Bev Glover Greenhouse Research Facility, University of Victoria, Victoria, BC, Canada). Plantlets were acclimated in a misting chamber for 3 weeks, then transplanted into 3.8 litre pots containing Sunshine Mix #4 supplemented with slow-release fertilizer (21.4 g l^{-1} Acer 21-7-14, 11.4 g l^{-1} dolomite lime, 2.9 g l^{-1} Micromax Micronutrients, and 1.1 g l^{-1} superphosphate 0-20-0) and grown for 3 months in an ambient humidity greenhouse compartment with supplemental light (16 h light, 8 h dark) at 22 °C with automated irrigation, unless stated otherwise. Leaves were indexed according to Larson and Isebrands (1971), starting at the first developing leaf with a maximum lamina length of 20 mm designated as leaf plastochron index (LPI) zero.

For high-light/UV-B exposure, 3-month-old plants were transferred from the greenhouse [average maximum photosynthetically active radiation (PAR): 253 μmol m^{-2} s^{-1} (LI-250A light meter, LI-COR Biosciences); average UV-B irradiance: 0.002 mW cm^{-2} (PMA 2200 Single-Input Radiometer, Solar Light)] and placed outdoors (south-east exposure immediately adjacent to the greenhouse) for 8 d during early August 2016 (maximum PAR: 1088 μmol m^{-2} s^{-1}; average UV-B irradiance: 0.09 mW cm^{-2}).

For luxuriant N fertilization (N-rich conditions) at 10 mM NH_4NO_3 (Pitre *et al.*, 2007b), misting chamber-acclimated plants were grown in 3.8 litre pots containing Sunshine Mix #2 (Sun Gro Horticulture), a peat-based growing mix, and without slow-release fertilizer. All plants were manually irrigated with a modified Long Ashton solution (Ehlting *et al.*, 2007), with NH_4NO_3 as the main N source (10 mM NH_4NO_3, 0.5 mM KNO_3, 0.9 mM $CaCl_2$, 0.3 mM $MgSO_4$, 0.6 mM KH_2PO_4, 42 μM K_2HPO_4, 10 μM Fe-EDTA, 2 μM $MnSO_4$, 10 μM H_3BO_3, 7 μM Na_2MoO_4, 0.05 μM $CoSO_4$, 0.2 μM $ZnSO_4$, 0.2 μM $CuSO_4$), and with fixed volumes that adequately saturated the growing mix 2–3 times per week, for 8 weeks.

Generation of transgenic poplar

PtNPF6.1 promoter and hairpin RNAi construct sequences were based on *P. trichocarpa* genome v3.1 and were amplified from *P. trichocarpa* (Nisqually-1) using Q5 High-Fidelity DNA polymerase (New England Biolabs), as recommended by the manufacturer. For the *PtNPF6.1::GUS* (β-glucuronidase) construct used to monitor *PtNPF6.1* expression via the *Escherichia coli uidA* (*GUS*) gene, a 1558 bp region upstream of *PtNPF6.1* was amplified from genomic DNA (forward primer, 5′-AGGATTTTACCGACGGATGA-3′; reverse primer, 5′-ACTCG TTGGCATGCTTTCTT-3′) and TA-cloned into the Gateway donor vector pCR8/GW/TOPO (Thermo Fisher Scientific). The sequence-validated donor insert was then recombined into the destination vector pMDC163 (Curtis and Grossniklaus, 2003) using an LR Clonase II reaction (Thermo Fisher Scientific) to produce a hygromycin-resistant promoter::*GUS* construct.

To assemble the *PtNPF6.1* hairpin RNAi cassette used to silence *PtNPF6.1* expression, a 305 bp fragment corresponding to the 5′-coding sequence of *PtNPF6.1* was amplified from cDNA isolated from young shoots (forward primer, 5′-GAGGATGGAAAGCTGCTCCT-3′; reverse primer, 5′-GCATTTTGGTGGACGTAAGC-3′). We designed the hairpin structure using the *P. trichocarpa* genome targeting Potri.002G029200 prior to the release of the INRA 717-1B4 genome (Zhou *et al.*, 2023), but note that the hairpin target sequences are almost identical to the *P. tremula* and *P. alba* paralogues present in the 717 *P. tremula* × *alba* hybrid used for genetic transformation [corresponding to PtXaTreH.02g025200 (two mismatches in the 79 bp hairpin) and PtXaAlbH.02g025600 (one mismatch), respectively]. Based on sequence identity, this fragment was expected to target both *PtNPF6.1* and its close paralogue *PtNPF6.2*, as the *P. trichocarpa* and *P. tremula* × *alba* versions of *NPF6.2* only have five mismatches to the hairpin probe each (Potri.005G23350 in the *P. trichocarpa* genome and PtXaTreH.05G181400, PtXaAlbH.05G183300 in the 717 *P. tremula* × *alba* genome). cDNA fragments were cloned sequentially into pKannibal (Wesley *et al.*, 2001) via restriction sites introduced through PCR amplification, as described by Coleman *et al.* (2008). In brief, the sense fragment was ligated via 5′-*Eco*RI and 3′-*Kpn*I sites, while the antisense fragment was ligated via 5′-*Bam*HI and 3′-*Hin*dIII sites. The entire hairpin RNAi cassette including the 35S cauliflower mosaic virus (CaMV) promoter and the octopine synthase (OCS) terminator was excised via the *Not*I sites and subcloned into the kanamycin-resistant binary vector pArt27 (Gleave, 1992).

The plant transformation constructs were verified by DNA sequencing and introduced into *Agrobacterium tumefaciens* C58 pMP90 via electroporation. Transgenic poplars were generated from hybrid aspen clone INRA 717-1B4, as described by Ma *et al.* (2004). In brief, callus cultures obtained after *Agrobacterium*-mediated transformation were transferred to shoot induction medium containing 0.2 μM thidiazuron and the appropriate selection antibiotic, and maintained at 22 °C under subdued light until regenerated shoots appeared. Shoots were micropropagated on half-strength MS medium supplemented with 0.5 μM IBA and 12.5 μg ml^{-1} hygromycin for *PtNPF6.1::GUS* lines or 50 μg ml^{-1} kanamycin for *PtNPF6.1* RNAi lines. Shoots that consistently rooted on medium containing selection antibiotic were confirmed to be transgenic via PCR screening. Four independent lines were selected for further analyses, and wild-type plants were used as controls for all experiments.

Expression analysis

Total RNA was isolated from leaves of greenhouse-grown plants using the method of Haruta *et al.* (2001). A 1 μg aliquot of DNase-treated RNA was used for cDNA synthesis with Superscript III reverse transcriptase (Thermo Fisher Scientific). *PtNPF6.1* transcript levels were analysed using quantitative real-time PCR (RT-PCR) on a CFX96 Real-Time PCR System (Bio-Rad). Reactions (15 μl) were prepared (in triplicate) using SsoFast EvaGreen supermix (Bio-Rad) according to the manufacturer's recommendations with 300 nM of each primer (forward primer, 5′-CATGCCAACGAGTTTGGTAAG-3′; reverse primer, 5′-CTTT CCATCCTCCAGTAGTTCG-3′) and 2 μl of cDNA template. Amplification conditions consisted of 95 °C for 30 s, followed by 40 cycles of 95 °C for 5 s and 55 °C for 5 s. cDNA abundance (ΔCt) was quantified relative to elongation factor 1β (Coleman *et al.*, 2008).

For *in situ* GUS staining, whole mounts (young leaves and roots) and hand-cut sections (leaf petiole from LPI 1, stem internodes 2 and 6 from the shoot tip, and roots) from 1-month-old greenhouse-grown plants were vacuum infiltrated in cold 90% acetone for 5 min and maintained in cold 90% acetone for 25 min. Sections were rinsed three times with 0.1 M $NaPO_4$ (pH 7.0) and incubated in X-Gluc solution {1 mM 5-bromo-4-chloro-3-indolyl-β-D-glucuronic acid, 0.5 mM $K_3[Fe(CN)_6]$, 0.5 mM $K_4[Fe(CN)_6]$, 0.1 M $NaPO_4$ (pH 7.0), 0.01% (v/v) Triton X-100} at 37 °C until the appearance of blue precipitate. Sections were cleared with 75% ethanol, as required, to remove chlorophyll. Cross-sections were mounted in water and imaged under bright-field settings using a Nikon Eclipse TE2000-U inverted microscope equipped with a Digital Sight DS-U1 camera and ACT-2U imaging software. Whole mounts were imaged using an Olympus SZX9 stereo microscope equipped with a DP72 camera and DP2-BSW imaging software.

Elemental analysis of carbon and nitrogen

Ground lyophilized leaves (LPI 9) from wild-type (WT) and transgenic lines were oven-dried overnight at 60 °C before use. Tin capsules

(Isomass Scientific) were packaged with ~5 mg of tissue and analysed on a FlashEA 1112 NC elemental analyser (Thermo Fisher Scientific). Total C and N concentrations were quantified.

Free amino acid analysis

Amino acid analysis was performed using phenyl isothiocyanate (Thermo Fisher Scientific) and a standard procedure at the British Columbia Ministry of Environment Analytical Laboratory (Victoria, BC, Canada). Free amino acids were extracted from 100 mg of ground lyophilized leaves (LPI 9) in 5 ml of 80% (v/v) methanol at 80 °C. The extraction was repeated three times, and the solvent was pooled for a total volume of 15 ml. In brief, amino acid standard H was added to 200 µl of extract, and the mixture was vacuum-dried and then resuspended in 20 µl of ethanol:water:triethylamine (2:2:1). Samples were redried and derivatized with 40 µl of ethanol:water:triethylamine:phenyl isothiocyanate (7:1:1:1), and incubated at room temperature for 20 min. Samples were then evaporated to dryness under vacuum, resuspended in 200 µl of phosphate buffer (pH 7.4), and separated on a Waters 2960 HPLC equipped with a Kinetex 2.6 µm C18 (100 Å) column (150×4.6 mm) and a photodiode array detector (254 nm). Elution was achieved via a gradient consisting of 93% eluent A at 0 min, changing to 50% eluent A by 15 min, where eluent A consisted of 1.8% sodium acetate and 0.05% triethylamine in water (pH 6.8) and eluent B was acetonitrile. The column was flushed with 80% acetonitrile and equilibrated for 5 min between injections.

Extraction and quantification of phenolic compounds

The extraction and analysis of anthocyanins was performed as described by Yoshida *et al.* (2015). Ground lyophilized leaves (50 mg) from LPI 6 and LPI 9 of WT and transgenic lines were extracted in 500 µl of acidic methanol [1% (v/v) concentrated aqueous HCl solution (37%) diluted in methanol] at room temperature for 16 h with gentle agitation. Water was added to the extract (1:1), followed by 1 ml of chloroform, after which the samples were centrifuged at 15 115 *g* for 15 min. The aqueous phase was isolated and measured at 530 nm on a Victor X5 multilabel plate reader (PerkinElmer) to quantify total anthocyanins. The aqueous phase (20 µl) was also separated on a Dionex UltiMate 3000 HPLC (Thermo) equipped with a Kinetex 2.6 µm C18 (100 Å) column (150×4.6 mm) (Phenomenex) and a photodiode array detector (520 nm). A linear gradient consisting of solvent A (4% formic acid in water) and solvent B (4% formic acid, 50% acetonitrile in water) was run at 15% B for 7.5 min, 45% B for 20 min, and 100% B for 24 min for a total of 27 min at a flow rate of 1 ml min^{-1} (Ma *et al.*, 2021). Cyanidin-3-glucoside was quantified using cyanidin-3-*O*-glucoside chloride (Carbosynth) as a standard.

For the extraction of condensed tannins and total soluble phenolics, ground lyophilized leaves (25 mg) from LPI 6 and LPI 9 of WT and transgenic lines were homogenized in 1.5 ml of methanol using a Precellys 24 tissue homogenizer (Bertin Instruments) at 3500 rpm for 45 s. Extracts were sonicated for 10 min and centrifuged at 15 115 *g* for 10 min. The extraction procedure was repeated twice more using 1 ml of 80% methanol, and all supernatants were pooled. Condensed tannins were measured using the butanol-HCl assay (Porter *et al.*, 1986; Gourlay and Constabel, 2019). In brief, reactions were heated at 95 °C for 30 min, equilibrated at room temperature, and measured at 550 nm on a Victor X5 multilabel plate reader (PerkinElmer). Condensed tannins were quantified using purified aspen condensed tannins to generate a standard curve. Quantification of total soluble phenolics was carried out using 20 µl of extract, 100 µl of Folin and Ciocalteu's phenol reagent (Sigma-Aldrich), and 500 µl of 20% Na_2CO_3 in a final volume of 1 ml. Reactions were incubated at room temperature for 45 min, centrifuged at 15 115 *g* for 1 min, and measured at 735 nm on a Victor X5 multilabel plate reader (PerkinElmer). Soluble phenolics were quantified using gallic acid (Sigma-Aldrich) to generate a standard curve.

Lignin analysis

Stems harvested ~2.5 cm above the soil from 2-month-old greenhouse-grown WT and transgenic plants were stripped of bark and air-dried. Segments of the basal stem with the pith removed were ground using a Wiley mill to pass through a 40 mesh sieve. The wood flour was Soxhlet-extracted with acetone at 70 °C for 16 h and oven-dried overnight at 50 °C before use. The lignin content was measured using a modified Klason lignin procedure (Porth *et al.*, 2013b). In brief, extractive-free wood flour was subjected to a swelling treatment for 1 h in 72% sulfuric acid, followed by secondary acid hydrolysis for 1 h in 4% sulfuric acid at 121 °C and 15 psi. The acid-insoluble fraction was determined as the dry weight of residue retained upon filtering the hydrolysate through a medium-coarseness fritted glass Gooch-type crucible. The acid-soluble fraction was measured spectrophotometrically at 205 nm using an extinction coefficient of 110 l g^{-1} cm^{-1}. Monolignol composition was determined using the thioacidolysis method described by Robinson and Mansfield (2009). In brief, 1 ml of reaction mixture (2.5% boron trifluoride etherate and 10% ethanethiol in dioxane) was added to 10 mg of oven-dried wood flour in screw-cap vials with a Teflon seal, blanketed with nitrogen, sealed, and heated at 100 °C for 4 h. Reaction products were extracted using dichloromethane and water, evaporated to dryness, and resuspended in dichloromethane. After derivatization with *N*, *O*-bis(trimethylsilyl) acetamide, 1 µl was analysed via GC using a Trace 1310 instrument equipped with a TraceGOLD 5MS column with helium as a carrier gas at a flow rate of 1 ml min^{-1} and a flame ionization detector provided with hydrogen at 35 ml min^{-1} and compressed air at 350 ml min^{-1}. The oven was initially held at 130 °C for 3 min following injection and was then ramped to 230 °C at 6.5 °C min^{-1}, held for 6 min, then ramped to 250 °C at 2.5 °C min^{-1}, and finally held for 10 min. Peaks corresponding to main diastereoisomers of derivatized lignin monomers were integrated and the total peak areas were used to calculate lignin monomer abundance.

The amount of cell-wall-bound *p*-hydroxybenzoate (*p*HB) was measured using alkaline hydrolysis, as described previously (Mottiar and Mansfield, 2022). In brief, 20 mg of extractive-free wood flour was subjected to alkaline hydrolysis in 1 ml of 2 M sodium hydroxide for 24 h at 30 °C. *o*-Anisic acid was added as an internal standard. After terminating the reactions with 100 µl of 72% sulfuric acid and filtering through a 0.45 µm syringe filter, the hydrolysates were measured by reverse-phase chromatography using a Dionex Summit HPLC (Thermo) equipped with a Symmetry C-18 column (Waters) maintained at 35 °C. A linear gradient of 5–45% of eluent A in eluent B was applied at a flow rate of 0.7 ml min^{-1} where eluent A was 0.1% trifluoroacetic acid in 70:30 acetonitrile:methanol and eluent B was 0.1% trifluoroacetic acid in water. Quantification of *p*HB was performed with a diode array detector set to 255 nm using a calibration curve prepared with analytical grade *p*-hydroxybenzoic acid.

Statistical analyses

Data were analysed using a Student's *t*-test in Excel, or an ANOVA in R. Details are included in the figure legends.

Results

PtNPF6.1 is evolutionarily distinct and lacks orthologues in many plant lineages

Potri.002G029200 from *P. trichocarpa* was previously identified as genetically associated with variation in syringyl lignin content

(Porth *et al.*, 2013a). Based on sequence comparisons with the Arabidopsis NPFs, Potri.002G029200 is most similar (~60% at the protein sequence level) to peptide transporters NPF8.1 and NPF8.2 (Dietrich *et al.*, 2004; Komarova *et al.*, 2008). However, phylogenetic reconstructions of NPFs revealed that this gene is evolutionarily distinct from NPF8.1 and NPF8.2, which belong to the NPF8/supergroup F clade (Léran *et al.*, 2014; von Wittgenstein *et al.*, 2014). Instead, Potri.002G029200 was assigned to subfamily NPF6 (Léran *et al.*, 2014), which includes the Arabidopsis nitrate transporters NPF6.2/NRT1.4 (Chiu *et al.*, 2004), NPF6.3/NRT1.1 (Tsay *et al.*, 1993), and NPF6.4/NRT1.3 (Tong *et al.*, 2016). We thus adopted the name PtNPF6.1. However, based on von Wittgenstein *et al.* (2014), NPF6 is a paraphyletic group comprising three distinct clades, designated supergroups B, E, and J (Fig. 1A). While the Arabidopsis nitrate transporters cluster in supergroup B, PtNPF6.1 belongs to the distinct supergroup J. Supergroup J orthologues are absent in Arabidopsis and many others plant lineages (von Wittgenstein *et al.*, 2014). We identified additional supergroup J NPF6 sequences in several eudicots, as well as in monilophytes (ferns), supporting early divergence during land plant evolution (Fig. 1A). Supergroup J members were not detected in bryophytes, lycopods, or gymnosperms, and were present in only approximately a third of all sampled angiosperm orders (Supplementary Fig. S1A). While supergroup J genes have been lost in many lineages, lineage-specific duplications occurred throughout angiosperm evolution, for example early within the Lamiales, and in multiple species in distinct families. In poplar, PtNPF6.2 is a closely related paralogue to PtNPF6.1. Taken together, it appears that supergroup J diverged early in land plant evolution and has been selectively retained or lost across plant lineages. To date, no supergroup J NPF6 member has been functionally characterized.

PtNPF6.1 is predominantly expressed in vascular tissues

To investigate the spatial expression of *PtNPF6.1*, a 1.6 kb fragment upstream of the *PtNPF6.1* coding sequence was cloned and fused to a GUS reporter, and introduced into hybrid poplar. Histochemical staining revealed that the strongest *PtNPF6.1::GUS* expression occurred in vascular tissues throughout the plant. In mature source leaves grown *in vitro*, expression was apparent in mesophyll cells, but was most pronounced in leaf veins (Supplementary Fig. S1B). A similar pattern was observed in young leaves (LPI 1) of 1-month-old greenhouse-grown plants, where *GUS* expression was strongest in the xylem (Fig. 1B, i and ii). In the stem at internode 2, *PtNPF6.1::GUS* expression was evident in developing secondary xylem (Fig. 1B, iii). At later stages in stem development, when xylem fibres, tracheids, and vessels had undergone secondary wall lignification and programmed cell death, GUS staining localized mainly at the vascular cambium and phloem (Fig. 1B, iv). A similar expression pattern was observed in mature roots with strong vascular expression (Fig. 1B, vi). GUS activity was only occasionally detected in the stele and in the root tips of some young roots (Fig. 1B, v; Supplementary Fig. S1B).

Nitrogen increases in transgenic poplar down-regulated in *PtNPF6*

To assess the functional role of PtNPF6.1, four independent transgenic poplar lines (three clonal replicates per line) expressing a hairpin RNAi construct targeting *PtNPF6.1* were generated and analysed. Owing to high sequence identity (97%), this RNAi construct probably suppresses both *PtNPF6.1* and the *PtNPF6.2* paralogue, hereafter referred to collectively as *PtNPF6*. Quantitative RT-PCR analysis showed significant reductions in *PtNPF6* transcript abundance in mature source leaves of lines 1 and 4. In lines 2 and 3, *PtNPF6* expression was suppressed by 20% and 60%, respectively, but these reductions were not statistically significant (Fig. 2A).

Elemental analysis showed that foliar N concentration in mature leaves increased by 30–40% in *PtNPF6* RNAi lines grown under a standard nutrient regime relative to the WT (Fig. 2B). This increase was significant in all lines except line 2, consistent with its weaker transcript suppression. In contrast, total foliar C concentration was unaffected by *PtNPF6* suppression.

To further characterize changes in N metabolism, free amino acid concentrations were quantified in mature leaves (LPI 9) of the WT and two RNAi lines: line 3 with moderate suppression and line 4 with strong suppression. Of the 20 standard amino acids, 14 were reliably quantified. Glutamic acid (Glu) and aspartic acid (Asp) levels accumulated to 2- to 3-fold higher in RNAi lines compared with the WT (Fig. 2C). Leucine (Leu) also showed a modest increase. In contrast, phenylalanine (Phe), which serves as a precursor for both protein and phenylpropanoid biosynthesis, was markedly reduced, with concentrations 5- and 1.6-fold lower than the WT in lines 3 and 4, respectively. Concentrations of other quantified amino acids were largely unchanged (Supplementary Table S2).

No visible differences in overall growth or development were observed among WT and RNAi lines after 3 months of greenhouse growth, indicating that elevated foliar N did not measurably affect vegetative growth under these conditions.

PtNPF6 suppression attenuates the accumulation of phenolic compounds under high-light and UV stress

Phenolic compounds, including anthocyanins, can accumulate in response to N deficiency and UV radiation (Dixon and Paiva, 1995; Ferreyra *et al.*, 2021). To test whether *PtNPF6* suppression influenced stress-induced phenolic accumulation, 3-month-old greenhouse-grown WT and *PtNPF6* RNAi lines were transferred outdoors during the summer to expose them to natural high-light/UV-B conditions. After 8 d, WT plants exhibited pronounced red pigmentation in young leaves, while

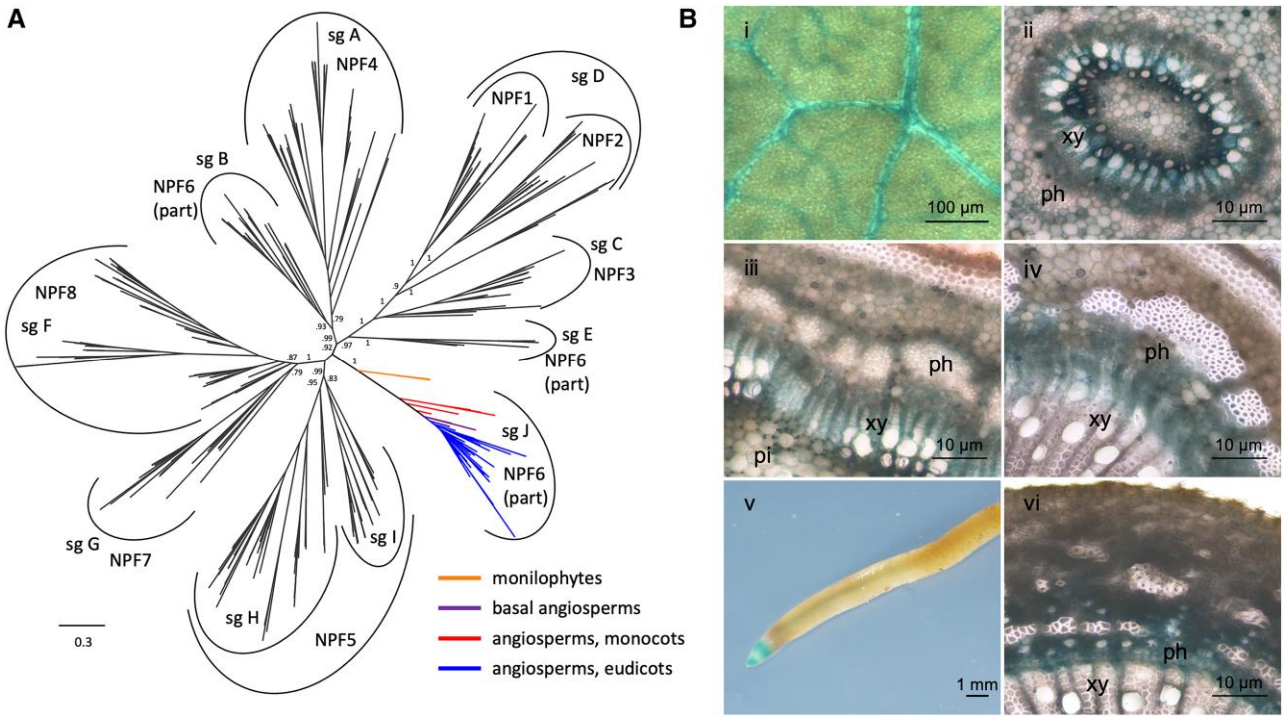

Fig. 1. Phylogenetic classification and expression profiling of PtNPF6.1. (A) An unrooted maximum likelihood phylogeny of the nitrate transporter 1/peptide transporter (NRT1/PTR) family (NPF) from land plants focusing on supergroup J. Complete NPF gene families from six species covering the major land plant lineages were used to reconstruct the NPF superfamily backbone. All sequences identified as supergroup J members were also included. Approximate likelihood-ratio test (aLRT) results for branches are shown if >0.7 and only for the core of the phylogeny up to branches leading into a labelled clade. Clades were labelled using nomenclature designated by von Wittgenstein *et al*. (2014) ('sg' for supergroup) and Léran *et al*. (2014) ('NPF'). Gene identifiers and database sources are given in Supplementary Table S1. Within clade sgJ, taxonomic groups are colour-coded as indicated. (B) Expression of *PtNPF6.1::GUS* in vascular tissue of 1-month-old greenhouse-grown transgenic poplar. (i) Leaf lamina of LPI 1. (ii) Cross-section of leaf petiole LPI 1. Cross-section of stem internode 2 (iii) and 6 (iv). (v) Whole mount of a young root with staining in the stele and root tip. (vi) Cross-section of mature root. ph, phloem; pi, pith; xy, xylem.

all four transgenic RNAi lines displayed visibly reduced colouration (Fig. 3A). Quantitative analysis showed that total anthocyanins were already reduced in the RNAi lines prior to outdoor exposure (Fig. 3B). After 4 d of high-light/UV-B exposure, both WT and RNAi lines increased anthocyanin production, but the RNAi lines accumulated only approximately half the anthocyanin levels observed in the WT. HPLC analysis of anthocyanin extracts revealed a prominent cyanidin-3-glucoside (Cy3G) peak at day 4, identified by comparision with an authentic standard. Cy3G in all RNAi lines was reduced by ~50% compared with the WT (Fig. 3C), consistent with the total anthocyanin measurements (Fig. 3B).

Condensed tannins, which constitute a major fraction of leaf phenolics in poplar (Mellway *et al*., 2009), were also strongly affected. Under greenhouse conditions, condensed tannin concentrations were 4–5 times lower in *PtNPF6* RNAi-suppressed lines compared with the WT. While WT plants showed increased condensed tannin accumulation in response to high light/UV-B, the response was significantly attenuated in the RNAi lines (Fig. 3D). Similarly, total soluble phenolics, assessed using the Folin–Ciocalteu assay, were reduced in *PtNPF6* RNAi lines both before and during outdoor exposure. Before outdoor exposure, *PtNPF6*-suppressed lines had significantly lower levels of soluble phenolics relative to the WT. After high-light/UV-B exposure, phenolic compounds accumulated in all genotypes; however, the RNAi lines accumulated significantly lower amounts than the WT (Fig. 3E). Together, these results indicate that *PtNPF6* suppression dampens phenolic accumulation under both baseline and stress-induced conditions.

Exogenous nitrogen alters lignin composition in *PtNPF6* RNAi lines

PtNPF6 was previously associated with variation in syringyl lignin content (Porth *et al*., 2013a), and high N availability is known to influence lignification in poplar (Pitre *et al*., 2007b). To test whether *PtNPF6* suppression altered lignin traits under N-rich conditions, WT plants and two *PtNPF6* RNAi lines were fertilized with a higher than standard ammonium nitrate regime (10 mM NH_4NO_3) for 8 weeks. Lignin composition was then quantified in the xylem tissues of the stems. Total lignin content did not differ between the WT and RNAi lines. However, small but significant changes in

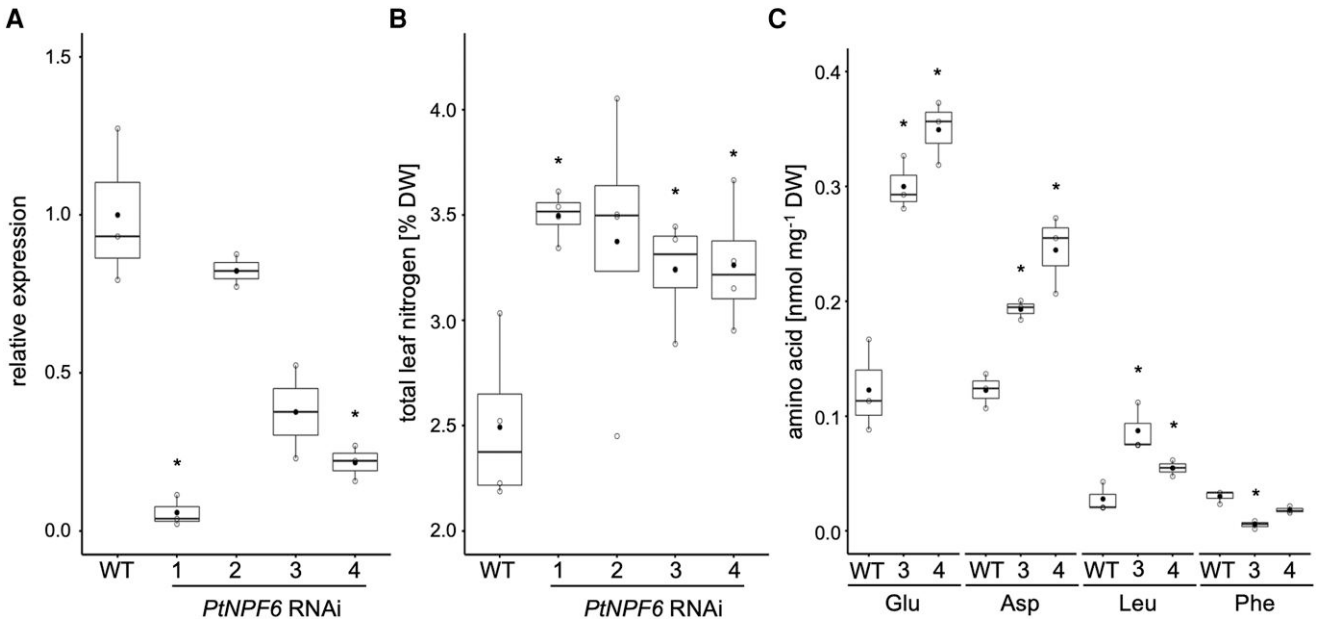

Fig. 2. Total nitrogen and free amino acids in leaves of *PtNPF6* RNAi trees. (A) Gene expression in mature, fully expanded leaves of *PtNPF6* RNAi lines relative to the wild type (WT). qPCR products were normalized to elongation factor 1β. Shown are data from three clonal replicates per line. (B) Total nitrogen concentrations in mature leaves (LPI 9) of the WT and RNAi lines. Shown are four clonal replicates per line. (C) Free amino acid concentrations in mature leaves (LPI 9) of the WT and RNAi lines. Shown are three clonal replicates per line. Only amino acids with significant differences are shown: Glu (glutamic acid), Asp (aspartic acid), Leu (leucine), and Phe (phenylalanine). The complete amino acid dataset is provided in Supplementary Table S2. The boxplots represent a 95% confidence interval and the horizontal bar inside the box is the median. The mean (filled circle) and individual biological replicates (open circles) are shown. Significant differences compared with the corresponding WT are based on a Student's *t*-test and are indicated by an asterisk ($P<0.05$).

lignin composition were observed. Both RNAi lines exhibited significant decreases in *p*-hydroxyphenyl (H) and syringyl (S) lignin, accompanied by an increase in guaiacyl (G) lignin, together resulting in a small, but significant reduction in the S:G ratio relative to the WT (Fig. 3F). In addition, RNAi lines showed a significant increase in *p*HB groups compared with the WT. Our results indicate that *PtNPF6* suppression alters lignin composition and associated wall-bound phenolics under high N availability.

Discussion

PtNPF6.1 probably functions at the interface of N and C homeostasis and within-plant N reallocation. This conclusion is supported by the predominant expression of *PtNPF6.1* in vascular tissues (Fig. 1B) and by the chemical phenotypes observed in RNAi-mediated suppression lines. RNAi lines exhibited increased total N concentration in mature leaves (Fig. 2B) alongside decreased phenolic compounds (Fig. 3). In addition, lignin composition was altered in the xylem of RNAi lines when grown under N-rich conditions (Fig. 3F). Although biochemical characterization will ultimately be required to identify the transported substrate(s), the opposing trends observed for N-containing compounds and non-N-containing phenolics are most parsimoniously explained by a role for PtNPF6.1 in the internal mobilization of N through the vascular tissues, probably involving export from mature source leaves.

The increase in foliar N concentrations observed in *PtNPF6* RNAi plants acts as a local signal that shifts the balance of C allocation away from phenolic biosynthesis towards protein production. These observations fit the C–nutrient balance hypothesis, which posits that plants allocate proportionally more C to growth-related processes under nutrient-rich conditions and to secondary metabolism under nutrient limitation (Bryant *et al.*, 1983). The generality of this hypothesis has been disputed (Hamilton *et al.*, 2001) and it is typically applied to whole-plant nutrient availability. In our study, N increased within mature leaves due to impaired within-plant N reallocation which coincided with decreased soluble phenolics in the same tissue, suggesting that N status can be sensed and responded to locally. One mechanistic link underlying this inverse relationship may be competition for Phe, a precursor to both proteins and phenylpropanoids (Jones and Hartley, 1999).

Consistent with this interpretation, *PtNPF6* RNAi lines accumulated elevated levels of Glu and Asp in mature leaves (Fig. 2C). These amino acids serve as amino donors for the conversion of prephenate to arogenate during Phe biosynthesis (Maeda and Dudareva, 2012), consistent with the observed increase in N concentration and decreased phenolics. In addition to Glu and Asp, glutamine (Gln) and asparagine (Asn) are products of N assimilation and are known to be transported via both

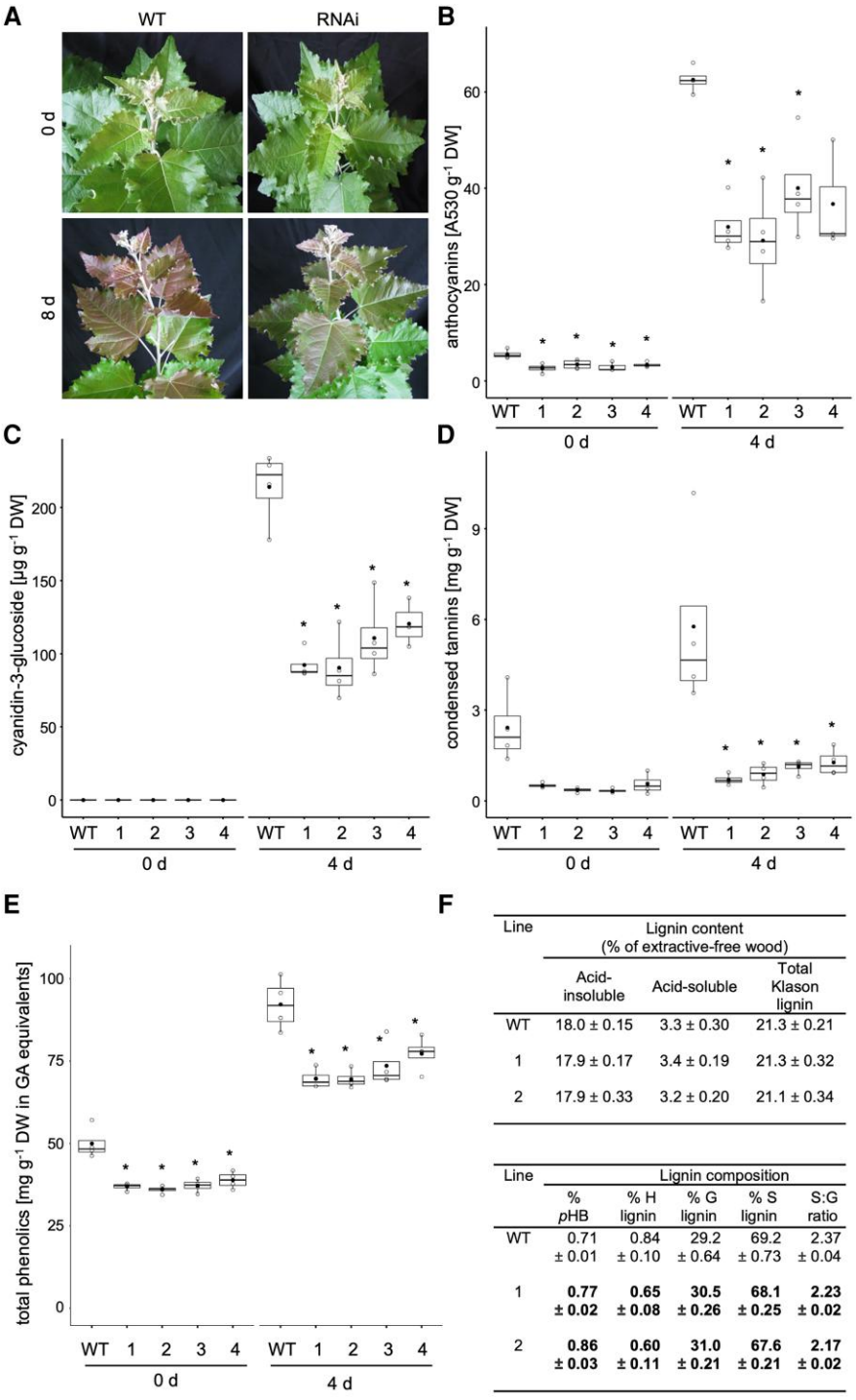

F

Line	Lignin content (% of extractive-free wood)		
	Acid-insoluble	Acid-soluble	Total Klason lignin
WT	18.0 ± 0.15	3.3 ± 0.30	21.3 ± 0.21
1	17.9 ± 0.17	3.4 ± 0.19	21.3 ± 0.32
2	17.9 ± 0.33	3.2 ± 0.20	21.1 ± 0.34

Line	Lignin composition				
	% *p*HB	% H lignin	% G lignin	% S lignin	S:G ratio
WT	0.71 ± 0.01	0.84 ± 0.10	29.2 ± 0.64	69.2 ± 0.73	2.37 ± 0.04
1	**0.77 ± 0.02**	**0.65 ± 0.08**	**30.5 ± 0.26**	**68.1 ± 0.25**	**2.23 ± 0.02**
2	**0.86 ± 0.03**	**0.60 ± 0.11**	**31.0 ± 0.21**	**67.6 ± 0.21**	**2.17 ± 0.02**

Fig. 3. Variation in phenolics in *PtNPF6* RNAi plants. (A) Phenotype of 3-month-old WT (left) and RNAi line 1 (right), a representative *PtNPF6* RNAi line before (0 d; top row) and after 8 d (bottom row) of outdoor high-light/UV-B exposure. (B, C) Anthocyanins measured as total anthocyanins (B) and cyanidin-3-glucoside (C) before (0 d) and during (4 d) high-light/UV-B exposure. (D) Condensed tannins before (0 d) and during (4 d) high-light/UV-B exposure. (E) Total soluble phenolics based on Folin and Ciocalteu's assay provided in gallic acid equivalents before (0 d) and during (4 d) high-light/UV-B exposure. The boxplots represent a 95% confidence interval and the horizontal bar inside the box is the median. The mean (filled circle) of four clonal replicates (open circles) is shown. Significant differences compared with the corresponding WT are based on a Student's *t*-test ($P<0.05$) and are indicated by an asterisk. All measurements at 4 d are significantly different from 0 d (ANOVA; $P<0.001$). (F) Lignin content and composition in stems of the WT and *PtNPF6* RNAi lines 1 and 2 grown under luxuriant nitrogen fertilization (10 mM ammonium nitrate). The mean and SEM are shown for four clonal replicates. Bold values indicate statistically significant differences from the WT based on a Student's *t*-test ($P<0.05$).

xylem and phloem (Hildebrandt *et al.*, 2015; Tegeder and Masclaux-Daubresse, 2018). Gln is the most abundant amino acid in poplar xylem sap and is transported to developing leaves (Cooke *et al.*, 2003; Rennenberg *et al.*, 2010). Its levels increase in xylem sap during seasonal transitions, such as during bud flush (Sauter and van Cleve, 1992). Given the strong vascular expression of *PtNPF6.1* in the leaves, stems, and roots, it is plausible that PtNPF6.1 contributes to the long-distance mobilization of organic N to support developing tissues.

High N availability has been shown to reduce the proportion of S lignin monomer content in poplar xylem (Pitre *et al.*, 2007b), consistent with the reduced S:G ratio observed in RNAi lines under N-rich conditions. Although the magnitude of these changes was modest, they corroborate the genetic association of *PtNPF6.1* with natural variation in S lignin content reported in a range-wide *P. trichocarpa* collection (Porth *et al.*, 2013a), where <5% of the trait variation in S lignin was explained by genetic variation at this locus (Porth *et al.*, 2013a).

Previous studies have shown that hybrid poplar grown under high N accumulates more H lignin units without changes in total lignin content when NH_4NO_3 is used as an N source (Pitre *et al.*, 2007b; Renström *et al.*, 2024). Consistent with this, we observed reduced H lignin in RNAi lines but no difference in total lignin content (Fig. 3F). The molecular basis linking N metabolism and lignin biosynthesis remains unresolved, but may involve N-containing compounds required for lignin biosynthesis, such as Phe and the methyl donor *S*-adenosylmethionine (SAM). Reduced availability of SAM or methionine could preferentially decrease S lignin biosynthesis, which requires two *O*-methylation reactions, thereby shifting lignin composition towards G units, which require only one *O*-methylation.

The increased abundance of ester-linked *p*HB groups observed in the transgenic RNAi lines is also noteworthy, as this too has been reported previously for N-fertilized hybrid poplar (Pitre *et al.*, 2007b; Goacher *et al.*, 2021), indicating that *p*HB production may also be related to N availability. In addition, the amounts of S lignin units and *p*HB groups were found to be inversely proportional to each other in natural populations of poplar and in metabolically engineered poplars (Mottiar and Mansfield, 2022; Mottiar *et al.*, 2023).

Together, these findings suggest that N status influences multiple aspects of cell wall phenolic chemistry, including both lignin composition and associated ester-linked modifications.

From an evolutionary perspective, PtNPF6.1 belongs to the phylogenetically distinct supergroup J of the NPF family (Fig. 1A), a group that is unevenly distributed across land plants. The early divergence of supergroup J and its frequent loss in many plant lineages suggests that its members fulfil specialized functions that are not universally required or that are partly redundant with other transport systems in lineages that have lost supergroup J.

Functional divergence within the NPF family is well documented, making it difficult to predict biochemical functions based on phylogenetic classification alone (von Wittgenstein *et al.*, 2014). An example is the Arabidopsis flavonol sophoroside transporter FST1 from subfamily NPF2 which belongs to the same subfamily as glucosinolate transporters (GTRs) NPF2.9, NPF2.10, and NPF2.11 (Grunewald *et al.*, 2020). Arabidopsis GTR1 is an evolutionary descendent of the phloem nitrate transporter NPF2.9/NRT1.9 (Wang and Tsay, 2011) and facilitates the long-distance transport of glucosinolates (Nour-Eldin *et al.*, 2012), which suggests that GTRs evolved via subfunctionalization (Jørgensen *et al.*, 2017). NPFs have been reported to transport other non-N-containing compounds, such as abscisic acid and gibberellin (Kanno *et al.*, 2012; Tal *et al.*, 2016; Binenbaum *et al.*, 2023). These findings suggest the potential for other yet to be identified NPF substrates.

In summary, suppression of *PtNPF6* revealed a role for this transporter in coordinating N availability with phenolic metabolism and lignin composition in poplar. These data support a model in which PtNPF6.1 contributes to internal N redistribution, thereby influencing C allocation between primary metabolism and secondary phenolic biosynthesis. Further biochemical characterization of PtNPF6.1 substrates and transport properties will be necessary to fully elucidate its role in balancing N and C homeostasis in woody perennials.

Supplementary data

The following supplementary data are available at *JXB* online.

Fig. S1. Detailed maximum likelihood phylogeny of NPF supergroup J and expression of *PtNPF6.1::GUS* in mature leaves and roots.

Table S1. Information and database identifiers for sequences used in phylogenetic reconstructions.

Table S2. Free amino acid concentrations in mature leaves of the wild type and *PtNPF6* RNAi lines.

Acknowledgements

Professor Carl J. Douglas (1955–2016) was instrumental in this research. He was a dedicated mentor, a generous colleague, and a treasured friend. This work is dedicated to his memory. We would like to thank Dr Lacey Samuels for her mentorship and contribution to this research. We would also like to thank Andre Bindon for the amino acid analysis, Brad Binges for managing the Bev Glover Greenhouse Research Facility, and Dr Barbara Ehlting for critical review of the manuscript.

Author contributions

LTT: design of the study with guidance from JE and SDM; LTT, YM, TI, ME, and SR: conducted the experiments; LTT, YM, BJH, and JE: analyzed the data; LTT and JE: wrote the original manuscript, and all authors contributed to the final version.

Conflict of interest

The authors declare there are no conflicts of interest.

Funding

This work was supported by individual Discovery Grants from the Natural Sciences and Engineering Research Council of Canada (NSERC) to JE, BJH, and SDM, and by Genome Canada, Genome BC, and others for the POPCAN Large-Scale Applied Research Project to JE and SDM. In addition, this work was supported by the DOE Great Lakes Bioenergy Research Center (DOE BER Office of Science DE-SC0018409) to SDM. We also acknowledge the generous support from the NSERC CREATE Working on Walls program to JE, SDM, and LTT, and postgraduate scholarships from NSERC and The University of British Columbia to LTT.

Data availability

This manuscript does not describe any primary data that require deposition in public repositories. Database sources for sequence data used in phylogenetic analyses are described in Supplementary Table S1.

References

Bai H, Euring D, Volmer K, Janz D, Polle A. 2013. The nitrate transporter (NRT) gene family in poplar. PLoS One **8**, e72126.

Benson DA, Cavanaugh M, Clark K, Karsch-Mizrachi I, Lipman DJ, Ostell J, Sayers EW. 2017. GenBank. Nucleic Acids Research **45**, D37–D42.

Binenbaum J, Wulff N, Camut L, *et al.* 2023. Gibberellin and abscisic acid transporters facilitate endodermal suberin formation in *Arabidopsis*. Nature Plants **9**, 785–802.

Bryant JP, Chapin FS III, Klein DR. 1983. Carbon/nutrient balance of boreal plants in relation to vertebrate herbivory. Oikos **40**, 357–368.

Cantón FR, Suárez MF, Cánovas FM. 2005. Molecular aspects of nitrogen mobilization and recycling in trees. Photosynthesis Research **83**, 265–278.

Castro-Rodríguez V, Cañas RA, de la Torre FN, Pascual MB, Avila C, Cánovas FM. 2017. Molecular fundamentals of nitrogen uptake and transport in trees. Journal of Experimental Botany **68**, 2489–2500.

Chang J-M, Di Tommaso P, Lefort V, Gascuel O, Notredame C. 2015. TCS: a web server for multiple sequence alignment evaluation and phylogenetic reconstruction. Nucleic Acids Research **43**, W3–W6.

Chiu C-C, Lin C-S, Hsia A-P, Su R-C, Lin H-L, Tsay Y-F. 2004. Mutation of a nitrate transporter, AtNRT1:4, results in a reduced petiole nitrate content and altered leaf development. Plant & Cell Physiology **45**, 1139–1148.

Coleman HD, Park J-Y, Nair R, Chapple C, Mansfield SD. 2008. RNAi-mediated suppression of *p*-coumaroyl-CoA 3′-hydroxylase in hybrid poplar impacts lignin deposition and soluble secondary metabolism. Proceedings of the National Academy of Sciences, USA **105**, 4501–4506.

Cooke JEK, Brown KA, Wu R, Davis JM. 2003. Gene expression associated with N-induced shifts in resource allocation in poplar. Plant, Cell & Environment **26**, 757–770.

Corratgé-Faillie C, Lacombe B. 2017. Substrate (un)specificity of Arabidopsis NRT1/PTR FAMILY (NPF) proteins. Journal of Experimental Botany **68**, 3107–3113.

Curtis MD, Grossniklaus U. 2003. A Gateway cloning vector set for high-throughput functional analysis of genes in planta. Plant Physiology **133**, 462–469.

Dietrich D, Hammes U, Thor K, Suter-Grotemeyer M, Flückiger R, Slusarenko AJ, Ward JM, Rentsch D. 2004. AtPTR1, a plasma membrane peptide transporter expressed during seed germination and in vascular tissue of *Arabidopsis*. The Plant Journal **40**, 488–499.

Dixon RA, Paiva NL. 1995. Stress-induced phenylpropanoid metabolism. The Plant Cell **7**, 1085–1097.

Ehlting B, Dluzniewska P, Dietrich H, *et al.* 2007. Interaction of nitrogen nutrition and salinity in Grey poplar (*Populus tremula* × *alba*). Plant, Cell & Environment **30**, 796–811.

Euring D, Bai H, Janz D, Polle A. 2014. Nitrogen-driven stem elongation in poplar is linked with wood modification and gene clusters for stress, photosynthesis and cell wall formation. BMC Plant Biology **14**, 391.

Ferreyra MLF, Serra P, Casati P. 2021. Recent advances on the roles of flavonoids as plant protective molecules after UV and high light exposure. Physiologia Plantarum **173**, 736–749.

Geβler A, Kopriva S, Rennenberg H. 2004. Regulation of nitrate uptake at the whole-tree level: interaction between nitrogen compounds, cytokinins and carbon metabolism. Tree Physiology **24**, 1313–1321.

Gleave AP. 1992. A versatile binary vector system with a T-DNA organisational structure conducive to efficient integration of cloned DNA into the plant genome. Plant Molecular Biology **20**, 1203–1207.

Goacher RE, Mottiar Y, Mansfield SD. 2021. ToF-SIMS imaging reveals that *p*-hydroxybenzoate groups specifically decorate the lignin of fibres in the xylem of poplar and willow. Holzforschung **75**, 452–462.

Goodstein DM, Shu S, Howson R, *et al.* 2012. Phytozome: a comparative platform for green plant genomics. Nucleic Acids Research **40**, D1178–D1186.

Gourlay G, Constabel CP. 2019. Condensed tannins are inducible antioxidants and protect hybrid poplar against oxidative stress. Tree Physiology **39**, 345–355.

Grunewald S, Marillonnet S, Hause G, Haferkamp I, Neuhaus HE, Veß A, Hollemann T, Vogt T. 2020. The tapetal major facilitator NPF2.8 is required for accumulation of flavonol glycosides on the pollen surface in *Arabidopsis thaliana*. The Plant Cell **32**, 1727–1748.

Guindon S, Dufayard J-F, Lefort V, Anisimova M, Hordijk W, Gascuel O. 2010. New algorithms and methods to estimate maximum-likelihood phylogenies: assessing the performance of PhyML 3.0. Systematic Biology **59**, 307–321.

Hamilton JG, Zangerl AR, DeLucia EH, Berenbaum MR. 2001. The carbon–nutrient balance hypothesis: its rise and fall. Ecology Letters **4**, 86–95.

Haruta M, Major IT, Christopher ME, Patton JJ, Constabel CP. 2001. A Kunitz trypsin inhibitor gene family from trembling aspen (*Populus tremuloides* Michx.): cloning, functional expression, and induction by wounding and herbivory. Plant Molecular Biology **46**, 347–359.

Hildebrandt TM, Nunes Nesi A, Araújo WL, Braun H-P. 2015. Amino acid catabolism in plants. Molecular Plant **8**, 1563–1579.

Huang N-C, Chiang C-S, Crawford NM, Tsay Y-F. 1996. *CHL1* encodes a component of the low-affinity nitrate uptake system in Arabidopsis and shows cell type-specific expression in roots. The Plant Cell **8**, 2183–2191.

Huang N-C, Liu K-H, Lo H-J, Tsay Y-F. 1999. Cloning and functional characterization of an Arabidopsis nitrate transporter gene that encodes a constitutive component of low-affinity uptake. The Plant Cell **11**, 1381–1392.

Jones CG, Hartley SE. 1999. A protein competition model of phenolic allocation. Oikos **86**, 27–44.

Jørgensen ME, Xu D, Crocoll C, Ernst HA, Ramírez D, Motawia MS, Olsen CE, Mirza O, Nour-Eldin HH, Halkier BA. 2017. Origin and evolution of transporter substrate specificity within the NPF family. eLife **6**, e19466.

Kanno Y, Hanada A, Chiba Y, Ichikawa T, Nakazawa M, Matsui M, Koshiba T, Kamiya Y, Seo M. 2012. Identification of an abscisic acid transporter by functional screening using the receptor complex as a sensor. Proceedings of the National Academy of Sciences, USA **109**, 9653–9658.

Komarova NY, Thor K, Gubler A, Meier S, Dietrich D, Weichert A, Suter Grotemeyer M, Tegeder M, Rentsch D. 2008. AtPTR1 and AtPTR5 transport dipeptides in planta. Plant Physiology **148**, 856–869.

Larbat R, Olsen KM, Slimestad R, Løvdal T, Bénard C, Verheul M, Bourgaud F, Robin C, Lillo C. 2012. Influence of repeated short-term nitrogen limitations on leaf phenolics metabolism in tomato. Phytochemistry **77**, 119–128.

Larson PR, Isebrands JG. 1971. The plastochron index as applied to developmental studies of cottonwood. Canadian Journal of Forest Research **1**, 1–11.

Lefort V, Longueville J-E, Gascuel O. 2017. SMS: smart model selection in PhyML. Molecular Biology and Evolution **34**, 2422–2424.

Léran S, Varala K, Boyer J-C, *et al.* 2014. A unified nomenclature of NITRATE TRANSPORTER 1/PEPTIDE TRANSPORTER family members in plants. Trends in Plant Science **19**, 5–9.

Lin S-H, Kuo H-F, Canivenc G, *et al.* 2008. Mutation of the *Arabidopsis NRT1.5* nitrate transporter causes defective root-to-shoot nitrate transport. The Plant Cell **20**, 2514–2528.

Luo J, Li H, Liu T, Polle A, Peng C, Luo Z-B. 2013. Nitrogen metabolism of two contrasting poplar species during acclimation to limiting nitrogen availability. Journal of Experimental Botany **64**, 4207–4224.

Ma C, Strauss SH, Meilan R. 2004. *Agrobacterium*-mediated transformation of the genome-sequenced poplar clone, Nisqually-1 (*Populus trichocarpa*). Plant Molecular Biology Reporter **22**, 311–312.

Ma D, Tang H, Reichelt M, Piirtola E-M, Salminen J-P, Gershenzon J, Constabel CP. 2021. Poplar MYB117 promotes anthocyanin synthesis and enhances flavonoid B-ring hydroxylation by up-regulating the flavonoid 3′,5′-hydroxylase gene. Journal of Experimental Botany **72**, 3864–3880.

Maeda H, Dudareva N. 2012. The shikimate pathway and aromatic amino acid biosynthesis in plants. Annual Review of Plant Biology **63**, 73–105.

Masclaux-Daubresse C, Daniel-Vedele F, Dechorgnat J, Chardon F, Gaufichon L, Suzuki A. 2010. Nitrogen uptake, assimilation and remobilization in plants: challenges for sustainable and productive agriculture. Annals of Botany **105**, 1141–1157.

Mellway RD, Tran LT, Prouse MB, Campbell MM, Constabel CP. 2009. The wound-, pathogen-, and ultraviolet B-responsive *MYB134* gene encodes an R2R3 MYB transcription factor that regulates proanthocyanidin synthesis in poplar. Plant Physiology **150**, 924–941.

Min X, Siddiqi MY, Guy RD, Glass ADM, Kronzucker HJ. 2000. A comparative kinetic analysis of nitrate and ammonium influx in two early-successional tree species of temperate and boreal forest ecosystems. Plant, Cell & Environment **23**, 321–328.

Mottiar Y, Mansfield SD. 2022. Lignin *p*-hydroxybenzoylation is negatively correlated with syringyl units in poplar. Frontiers in Plant Science **13**, 938083.

Mottiar Y, Karlen SD, Goacher RE, Ralph J, Mansfield SD. 2023. Metabolic engineering of *p*-hydroxybenzoate in poplar lignin. Plant Biotechnology Journal **21**, 176–188.

Nour-Eldin HH, Andersen TG, Burow M, Madsen SR, Jørgensen ME, Olsen CE, Dreyer I, Hedrich R, Geiger D, Halkier BA. 2012. NRT/PTR transporters are essential for translocation of glucosinolate defence compounds to seeds. Nature **488**, 531–534.

One Thousand Plant Transcriptomes Initiative. 2019. One thousand plant transcriptomes and the phylogenomics of green plants. Nature **574**, 679–685.

Parker JL, Newstead S. 2014. Molecular basis of nitrate uptake by the plant nitrate transporter NRT1.1. Nature **507**, 68–72.

Paungfoo-Lonhienne C, Lonhienne TGA, Rentsch D, Robinson N, Christie M, Webb RI, Gamage HK, Carroll BJ, Schenk PM, Schmidt S. 2008. Plants can use protein as a nitrogen source without assistance from other organisms. Proceedings of the National Academy of Sciences, USA **105**, 4524–4529.

Payne RME, Xu D, Foureau E, *et al.* 2017. An NPF transporter exports a central monoterpene indole alkaloid intermediate from the vacuole. Nature Plants **3**, 16208.

Pitre FE, Cooke JEK, Mackay JJ. 2007a. Short-term effects of nitrogen availability on wood formation and fibre properties in hybrid poplar. Trees **21**, 249–259.

Pitre FE, Pollet B, Lafarguette F, Cooke JEK, MacKay JJ, Lapierre C. 2007b. Effects of increased nitrogen supply on the lignification of poplar wood. Journal of Agricultural and Food Chemistry **55**, 10306–10314.

Plavcová L, Hacke UG, Almeida-Rodriguez AM, Li E, Douglas CJ. 2013. Gene expression patterns underlying changes in xylem structure and function in response to increased nitrogen availability in hybrid poplar. Plant, Cell & Environment **36**, 186–199.

Porter LJ, Hrstich LN, Chan BG. 1986. The conversion of procyanidins and prodelphinidins to cyanidin and delphinidin. Phytochemistry **25**, 223–230.

Porth I, Klapšte J, Skyba O, *et al.* 2013a. Genome-wide association mapping for wood characteristics in *Populus* identifies an array of candidate single nucleotide polymorphisms. New Phytologist **200**, 710–726.

Porth I, Klápště J, Skyba O, Lai BSK, Geraldes A, Muchero W, Tuskan GA, Douglas CJ, El-Kassaby YA, Mansfield SD. 2013b. *Populus trichocarpa* cell wall chemistry and ultrastructure trait variation, genetic control and genetic correlations. New Phytologist **197**, 777–790.

Razal RA, Ellis S, Singh S, Lewis NG, Towers GHN. 1996. Nitrogen recycling in phenylpropanoid metabolism. Phytochemistry **41**, 31–35.

Rennenberg H, Wildhagen H, Ehlting B. 2010. Nitrogen nutrition of poplar trees. Plant Biology **12**, 275–291.

Renström A, Choudhary S, Gandla ML, Jönsson LJ, Hedenström M, Jämtgård S, Tuominen H. 2024. The effect of nitrogen source and levels on hybrid aspen tree physiology and wood formation. Physiologia Plantarum **176**, e14219.

Robinson AR, Mansfield SD. 2009. Rapid analysis of poplar lignin monomer composition by a streamlined thioacidolysis procedure and near-infrared reflectance-based prediction modeling. The Plant Journal **58**, 706–714.

Sauter JJ, van Cleve B. 1992. Seasonal variation of amino acids in the xylem sap of 'Populus × canadensis' and its relation to protein body mobilization. Trees **7**, 26–32.

Tal I, Zhang Y, Jørgensen ME, *et al.* 2016. The Arabidopsis NPF3 protein is a GA transporter. Nature Communications **7**, 11486.

Tegeder M, Masclaux-Daubresse C. 2018. Source and sink mechanisms of nitrogen transport and use. New Phytologist **217**, 35–53.

Thompson JD, Higgins DG, Gibson TJ. 1994. CLUSTAL W: improving the sensitivity of progressive multiple sequence alignment through sequence weighting, position-specific gap penalties and weight matrix choice. Nucleic Acids Research **22**, 4673–4680.

Tong W, Imai A, Tabata R, Shigenobu S, Yamaguchi K, Yamada M, Hasebe M, Sawa S, Motose H, Takahashi T. 2016. Polyamine resistance is increased by mutations in a nitrate transporter gene *NRT1.3* (*AtNPF6.4*) in *Arabidopsis thaliana*. Frontiers in Plant Science **7**, 834.

Tsay Y-F, Schroeder JI, Feldmann KA, Crawford NM. 1993. The herbicide sensitivity gene *CHL1* of Arabidopsis encodes a nitrate-inducible nitrate transporter. Cell **72**, 705–713.

Tsay Y-F, Chiu C-C, Tsai C-B, Ho C-H, Hsu P-K. 2007. Nitrate transporters and peptide transporters. FEBS Letters **581**, 2290–2300.

Vogt T. 2010. Phenylpropanoid biosynthesis. Molecular Plant **3**, 2–20.

von Wittgenstein NJ, Le CH, Hawkins BJ, Ehlting J. 2014. Evolutionary classification of ammonium, nitrate, and peptide transporters in land plants. BMC Evolutionary Biology **14**, 11.

Wang Y-Y, Tsay Y-F. 2011. *Arabidopsis* nitrate transporter NRT1.9 is important in phloem nitrate transport. The Plant Cell **23**, 1945–1957.

Wang Y-Y, Hsu P-K, Tsay Y-F. 2012. Uptake, allocation and signaling of nitrate. Trends in Plant Science **17**, 458–467.

Wesley SV, Helliwell CA, Smith NA, *et al.* 2001. Construct design for efficient, effective and high-throughput gene silencing in plants. The Plant Journal **27**, 581–590.

Yoshida K, Ma D, Constabel CP. 2015. The MYB182 protein down-regulates proanthocyanidin and anthocyanin biosynthesis in poplar by repressing both structural and regulatory flavonoid genes. Plant Physiology **167**, 693–710.

Zhou R, Jenkins JW, Zeng Y, *et al.* 2023. Haplotype-resolved genome assembly of *Populus tremula* × *P. alba* reveals aspen-specific megabase satellite DNA. The Plant Journal **116**, 1003–1017.